IEEE Access
Multidisciplinary | Rapid Review | Open Access Journal

Received December 26, 2019, accepted January 11, 2020, date of publication January 17, 2020, date of current version January 30, 2020.

Digital Object Identifier 10.1109/ACCESS.2020.2967651

Compact Eight-Element Antenna Array for Triple-Band MIMO Operation in 5G Mobile Terminals

HONGWEI WANG, RUIHENG ZHANG, YONG LUO, AND GUANGLI YANG

Shanghai Institute for Advanced Communication and Data Science, Shanghai University, Shanghai 200444, China
Key Laboratory of Specialty Fiber Optics and Optical Access Networks, Shanghai University, Shanghai 200444, China

Corresponding author: Guangli Yang (guangli.yang@shu.edu.cn)

This work was supported by the Shanghai Eastern Scholarship.

ABSTRACT In this paper, we have introduced a compact eight-element antenna array for triple-band MIMO (multi-input multi-output) operation in 5G (fifth generation) mobile terminals, which consists of two symmetric four-element sub-arrays disposed, respectively, along two long side-edges of the system ground plane of the mobile terminal. This antenna element can operate at two dual-wideband of 3250-3820 MHz and 4790-6200 MHz with three resonance frequencies which can fully cover 5G NR (New Radio) Band-N78 (3300-3800 MHz), China 5G-Band of 4800-5000 MHz and LTE Band-46 (5150-5925 MHz). The main parameters that characterize the performance of the proposed MIMO antenna system, such as bandwidth, reflection coefficient, isolation (more than 10.5 dB), total radiation efficiency (more than 43%), ECC (envelope correlation coefficient, less than 0.12) and CC (channel capacity, 34.9-37.6 bps/Hz), are analyzed and presented in this paper. Besides, the effects of single-hand and dual-hand on performance of the MIMO antenna system are also discussed. The structure of antenna element is only 15 mm $\times$ 3 mm (0.175 $\lambda_0 \times$ 0.035 λ_0, λ_0 is the free-space wavelength at the frequency of 3.5 GHz) with a very small ground clearance of 13 mm $\times$ 2 mm on the main board of the proposed mobile terminal. The antenna system has the possibility to be used in 5G mobile terminals with triple-band operation, narrow frame and large display. The corresponding antennas prototype is fabricated and measured; and a quite good agreement between simulation and measurement is obtained.

INDEX TERMS Compact antennas, triple-band antennas, eight-element antenna array, MIMO system, 5G mobile terminal.

I. INTRODUCTION

In the coming era of 5G (fifth generation) mobile communication, the world is in full swing with antenna designs for mobile terminals and base stations with higher transmission rate, shorter latency and higher access rate, which have absolute advantages over the current 4G (fourth generation) system. The applications of 5G mobile communications comes from various areas such as cars, VR (Virtual Reality), cloud-powered apps and IoT (Internet of Things) etc., [1]. As we all know that improving spectral efficiency can effectively increase communication capacity. However, the spectrum resources are very precious and limited. Another approach is to use multi-input multi-output (MIMO) antennas in the mobile terminals to achieve higher data throughput, this is actually the most popular way adopted in 5G mobile communication. As for the 5G's operation bands, about four years ago, the International Telecommunications Union's WRC-15 reached agreements and identified new spectrum for mobile communications for International Mobile Telecommunications, and made the part of the C-Band (3400-3600 MHz) available for mobile broadband on a global basis as well as identified additional spectrum in some countries in the frequency bands of 3300-3400 MHz, 3600-3700 MHz and 4800-4990 MHz [2]. Additionally, Ministry of Industry and Information Technology of the People's Republic of China has identified that the 3300-3400 MHz, 3400-3600 MHz (LTE band 42) and 4800-5000 MHz as the operation bands of 5G system [3]. Besides, 3400-3800 MHz (LTE band 42/43) has also been recognized by many countries, such as European Union (EU), as a pioneer to realize 5G MIMO system [4]. The 3GPP has also announced that the 5G NR (New Radio) band: N78 (3300-3800 MHz) for the sub-6 GHz application [5]. In addition, LTE Band-46 of

The associate editor coordinating the review of this manuscript and approving it for publication was Giorgio Montisci.

5150-5925 MHz has also considerable competitive potential to be employed in the 5G mobile terminals for MIMO applications even though it is so far an unlicensed operation band [6]. Therefore, to cover all the above 5G operation bands for seamless Internet access globally, it is better to design MIMO antenna systems that can simultaneously cover the triple-band of 3300-3800 MHz, 4800-5000 MHz and 5150-5925 MHz. In the past, the multi-band antennas designed for mobile terminals that can support the low band: GSM (824-960 MHz) and the high band: DCS/PCS/UMTS (1710-2170 MHz) [7]–[11], even the lower band: LTE700 (698-787 MHz) and the higher band: LTE2300/2500 (2305-2690 MHz) [12]–[16]. In recent years, it is interesting to note that many literatures have begun to study the sub-6 GHz (especially focused on 3.5 GHz band of 3400-3600 MHz) MIMO antenna systems designed in 5G mobile devices [17]–[39]. In order to achieve multiband MIMO operation, there are several mobile terminal antenna arrays designed for 5G sub-6 GHz massive MIMO have also been reported [30]–[39]. However, amid these designs, most of them only focused on improvement of one of the parameter indicators in MIMO antenna systems. And, few literatures have simultaneously studied the improvement of two or more of the parameter indicators. For example, the literature [20]–[24] and [25] have proposed several good solutions to improve isolation between antenna elements in MIMO multi-antenna systems. And, the literature [20] and [21] therein applied self-isolated antenna element and self-decoupled antenna pairs techniques to realize high isolation, respectively. The literature [22] and [23] therein applied the orthogonal polarization diversity technique based on different excitation modes to obtain high isolation, while the literature [24] applied multimode decoupling technique to enhance isolation of the antenna elements. And the use of the tiny neutralizing line technique to achieve higher isolation has also been investigated in the literature [25]. Although those approaches mentioned above can effectively improve the isolation between antenna elements, some of which are even more than 17 dB, they only considered the case of single-band MIMO operation. Certainly, the literature [26]–[28] and [29] have studied the design of dual-band MIMO antennas in 5G smartphones. However, since the antennas in [26] and [27] are all printed on the inner surface of side-edge frame of the smartphones and are located at the upper and lower sides of the frame perpendicularly placed to the system substrate of the smartphones, this needs to be realized based on the fixed width of the frame of the mobile phones, which limits the realization of ultra-thin design of the future 5G mobile phones. The literature [28] and [29] therein requires large space or large ground clearance for embedding the antenna element or complicated decoupling structure, respectively, to realize the design of the MIMO antennas, and they have no capacity to cover the typical 5G bands mentioned above. Furthermore, the MIMO antennas in literature [30] and [31] show that they can realize compact and low-profile structure, that is: two-antenna building block is formed by two gap-coupled loop antennas having asymmetrically mirrored structures with respect to the system ground plane and 3D folded loop antenna structures, respectively, but they also considered the single-band MIMO operation with accepted performance and were not suitable for mobile terminals with narrow frame. In addition, in the literature [32]–[36] and [37], although the antennas are not printed on the frame of the smartphones, its occupied areas of the ground clearance are relatively large, especially in the literature [32] and [33]. Large ground clearance or ground slits are required to realize the antenna design, which largely affects the placement of other electronic components or functional modules in practical environment of the mobile terminals. And in the literature [34], the layout of MIMO antennas can easily introduce a new issue of its coexistence with current 4G LTE and other antennas. As for antennas in the literature [35], [36] and [37], although the ground clearance becomes smaller and more antennas (10- or 16-antennas) are embedded in the smartphones to achieve higher channel capacity, they only considered the case of single-band MIMO operation. It would be better if the ground clearance could be reduced and the antennas could realize multi-band MIMO operation. Heretofore, few literatures have comprehensively considered the miniaturization, multi-band operation and small PCB ground clearance of the MIMO antenna systems, and the possible problems of spatial coexistence between MIMO antennas with other electrical components in practical terminals.

Due to the limited space in mobile terminals, however, how to achieve small-size or low-profile MIMO antennas with multi-band operation has become a critical challenge for future 5G mobile terminal products. In this paper, we proposed an 8×8 MIMO antenna system with the advantages of small dimensions (only $0.152\ \lambda_0 \times\ 0.023\lambda_0$ and $0.175\lambda_0 \times\ 0.035\lambda_0$, λ_0 is the free-space wavelength at the frequency of 3.5 GHz) in horizontal and vertical planes of the mobile terminal and triple-band (3300-3800 MHz, 4800-5000 MHz and 5150-5925 MHz) operations, both of these two characteristics are better than those proposed in literature [17]–[39] when considering the MIMO antenna system combined with configuration of mobile terminal from the perspective of comprehensive parameter or performance, which has the great potential to meet the requirements of the future ultra-thin 5G mobile terminals with narrow-frame and wide-screen.

In this work, simulated results of the proposed eight-element antenna array are obtained using electromagnetic simulation software CST Studio Suite version 2018 [44] and the full-wave electromagnetic field simulator HFSS version 19.2 [45], the corresponding measured results were obtained by vector network analyzer (VNA, Keysight's E5071C) and ETS AMS 8500 microwave chamber.

II. STRUCTURE OF THE PROPOSED COMPACT EIGHT-ELEMENT TRIPLE-BAND ANTENNA ARRAY

The schematic of the proposed compact eight-element triple-band antenna array is shown in Fig.1. As shown in Fig.1 (a),

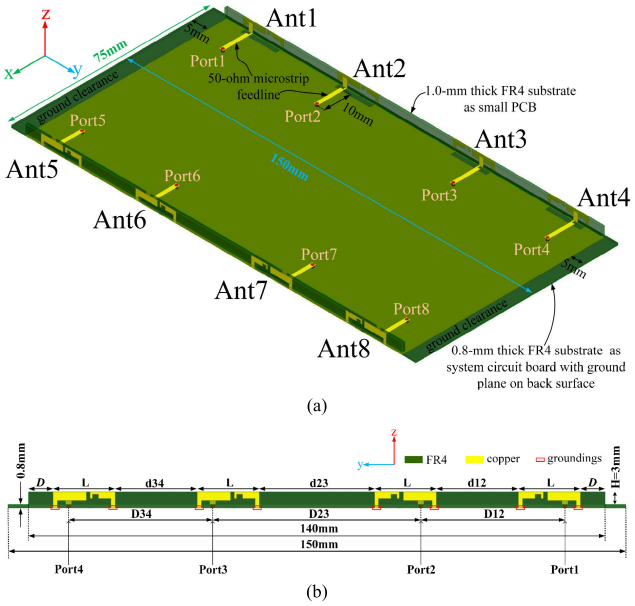

FIGURE 1. Perspective view, side view of the proposed eight-element triple-band antenna array. (a) perspective view, and (b) side view.

two same four-antenna arrays are symmetrically placed along the two long edges of the system substrate of mobile terminal. The dimension of the system substrate is the standard phone size of 150 mm × 75 mm × 0.8 mm. The system ground plane printed on the back of the system substrate with dimension of 140 mm × 75 mm. In addition, two small substrates as small PCBs (Printed Circuit Board) are placed perpendicularly on the system substrate and adjacent to the two long edges of the system substrate, respectively, with same dimensions of 140 mm × 3 mm × 1 mm. Both the system substrate and small substrate are all double-sided FR4 (relative permittivity 4.4 and loss tangent 0.02). In order to accommodate two LTE/WWAN antennas for the 2G/3G/4G operation, two rectangular ground-clearance areas (with the same dimension of 75 mm × 5 mm) at the top and bottom edges of the system ground plane has been reserved. Each antenna (Ant. 1-Ant. 8 shown in Fig.1 (a)) is fed with a 50-ohm microstrip line and a SMA connector through via-hole from the back side of the system substrate. Furthermore, in order to clearly depict the arrangement of the proposed 8-antenna array and the distances between antenna elements therein, a side view of the 4-antenna linear sub-array is given in Fig. 1(b). The values for the parameters in Fig. 1(b) are: L = 15 mm, H = 3 mm, D = 6 mm, d34 = d12 = 20 mm, d23 = 28 mm, D34 = D12 = 35 mm and D23 = 50.5 mm, where, L and H denotes the length of antenna element and the height of the small PCB as well as the height of the antenna element, respectively, d23, d34 and d12 denotes distances between Ant. 2 and Ant. 3, Ant. 3 and Ant. 4, Ant. 1 and Ant. 2, respectively. And, D23, D34 and D12 denotes distances between Port 2 and Port 3, Port 3 and Port 4, Port 1 and Port 2, respectively.

The geometry and detailed dimensions of the proposed triple-band antenna element are shown in Fig. 2. The antenna element has one coupled-fed arm (CFA, the segment DEF) and one parasitic arm (PA, the segment GHIJ) (see outer branches or outer surface of the small PCB in Fig. 2) resonating at 3.5 GHz and 5.5 GHz, respectively, meanwhile, the open-slot (OS, the area MDKLJN) is formed by cutting two slots on the ground plane (see back surface of system circuit board in Fig. 2). The coupled-fed strip (the segment ABC) is placed at the inner surface of the small PCB as shown in Fig. 2 (see inner surface of small PCB). A 10-mm length and 1.5-mm width microstrip feedline (the segment PA) having a characteristic impedance of 50-ohm is applied to feed the antenna element. The proposed antenna array has advantages of small volume, triple-band operation and simple structure for fabrication.

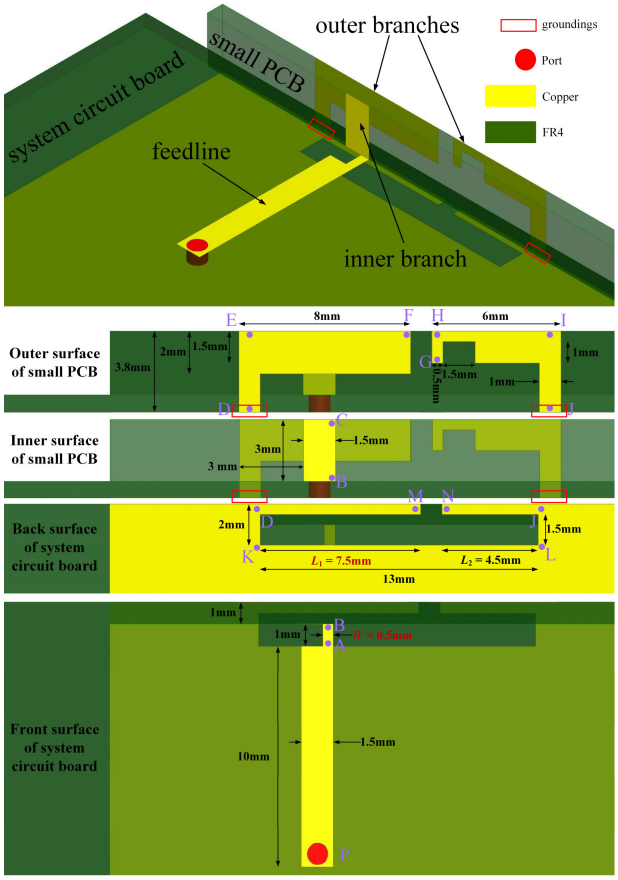

FIGURE 2. Perspective view, side view, back view and front view of the proposed triple-band antenna element structure with detailed dimensions.

III. SIMULATED RESULTS AND ANALYSIS

In this section, the simulated results, such as S-parameters, bandwidth, total efficiency of the proposed compact eight-element triple-band antenna array are presented. Also, to better understand the antenna design principle, the antenna design's evolution steps from beginning to the final stage,

current distributions at critical frequencies, antenna location as well as hand impact to the performance are presented and discussed.

A. EVOLUTION OF ANTENNA ELEMENT DESIGN

To better understand the design process or design steps of the antenna element, six different cases of antenna element based on direct-fed (Case I) and coupled-fed (Case II, III, IV, V, VI) structures are discussed in this sub-section, as shown in Fig. 3. Practically, the shape and size of the mobile terminal antenna are governed by the antenna body and available space. Therefore, this design skillfully combines CFA, PA and OS to form three distinct excitation modes with reduced dimensions as well as relative wide bandwidth.

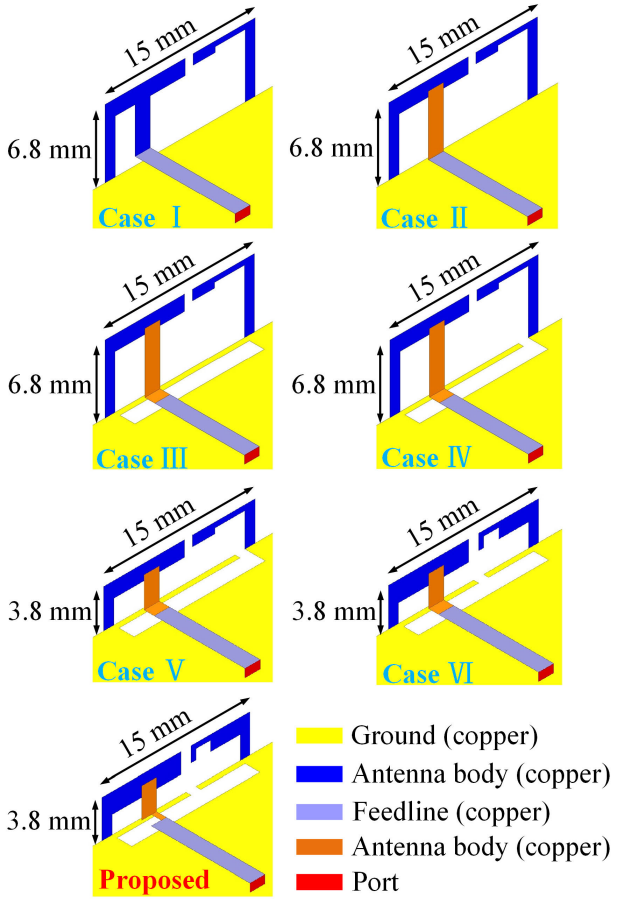

FIGURE 3. Evolution of antenna element design.

When only the mechanism of the coupled-fed structure is studied in this paper, the antenna design starts from Case II with a CFA to create resonance at 3.15 GHz and PA at 4.75 GHz. The coupled feed is used because direct feed does not work for this case, that is, one can see from Fig. 4 (Case I), the antenna element with direct feed can only generate one resonance at 3.9 GHz with limited bandwidth in the band of 3-6.5 GHz and cannot effectively excite the PA mode for wider bandwidth operation. As shown in Fig. 4, for Case II, two resonances are created but not enough to cover triple band, the idea is to create a third mode to expend bandwidth using slot on the ground plane which starts from Case III with a narrow slot, and an 0.5-wavelength slot mode has been excited at 6.9 GHz. However, the bandwidth created by the third mode plus the two previously existing bandwidths still does not cover the required triple-band, the antenna needs to be further optimized. In Case IV, an open area is cut at area close to the PA grounding leg, an OS resonance is created at 3.9 GHz at this stage, and to move it higher toward the band of 4.8-5.925 GHz. In Case V, the antenna height is reduced from 6.8 to 3.8 mm which is also the main purpose of this paper, the third resonance now works at 4.5 GHz but still need to shift higher within the band of interest, this can be done by moving slot cut area (by changing the L_1) toward CFA grounding leg direction to reduce the slot effective operation length. In Case VI, based on the resonance mode of the previous step, by moving the slot cut area toward the CFA grounding leg direction and finely changing the structures of the CFA and PA, the resonant impedance matching of the antenna element is optimized, as shown in Fig. 3 (Case VI) and the corresponding S_{11} is shown in Fig. 4 (Case VI). Furthermore, by adjusting the width of the coupled-fed structure (the width of segment AB is W in Fig. 2), the matching of the antenna element in the required triple-band is improved, especially in the band of 4.8-5 GHz, which resulting in a dual wide-bandwidth with reflection coefficient are all less than -6 dB, finally the proposed antenna design is completed, as shown in Fig. 4 (Proposed).

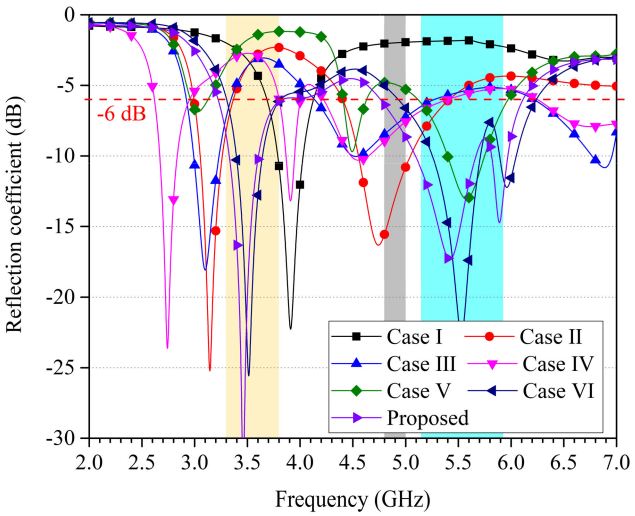

FIGURE 4. Simulated reflection coefficients in the evolution of antenna element design.

The corresponding reflection coefficients in the evolution of the antenna element are all shown in Fig. 4. From the simulated S_{11} of the proposed antenna element, three clear modes, CFA mode for band of 3.3-3.8 GHz, PA mode and OS mode for bands of 4.8-5 GHz and 5.15-5.925 GHz are created to cover all the desired bands. The merit of the antenna

design is that the quarter-wavelength open-slot (OS) mode can be excited without additional feeding structure, it not only creates additional bandwidth but also enhances the CFA and PA bandwidths a little bit, thus forming a dual-wideband antenna element structure with three resonant modes and reduced dimensions, which is used to form the compact triple-band 8 × 8 MIMO system.

B. WORKING PRINCIPLE OF ANTENNA ELEMENT

To further understand the working principle of the proposed compact triple-band antenna element, the current distribution on each mode can give more insights. In this case, the 10 mm 50-ohm microstrip feedline is removed and the antenna element is excited directly (zero-phase point) for clear current distribution study. This is because the original feeding line adds additional phase to antenna at the three resonant frequency modes, which makes current analysis more complicated. However, this 50-ohm microstrip feedline does not have effects on the entire antenna array and MIMO system. The reason to include a long feedline is mainly for the purpose of experiment convenience, as the 50-ohm feedlines can be fed through the SMA connectors to directly feed the antenna body. To make sure antenna's reflection coefficients and total radiation efficiencies are essentially the same at the cases with and without the 50-ohm feedline, they are plotted and compared in Fig. 5(a) and Fig. 5(b), respectively.

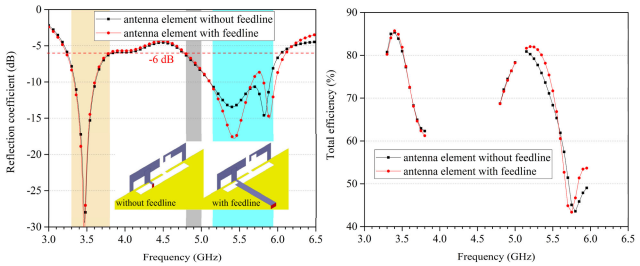

FIGURE 5. Simulated results of the proposed antenna element with or without feedline. (a) reflection coefficients and (b) total radiation efficiencies.

To further illustrate the three resonant modes of the antenna element, the simulated equivalent vector surface distributions at 3500 MHz, 5500 MHz and 5900 MHz are respectively displayed in Fig. 6 (top, middle and bottom). For the resonant frequency point of 3.5 GHz, the current path mainly focuses on the left outer branch which can contribute a 0.25-wavelength resonant mode (CFA works for 0.25-wavelength coupled-loop mode, the length (L) of the current path is: $L_{\mathrm{ABCFEDKO}} = 20.8$ mm $\approx 0.24\ \lambda_0$, λ_0 is the free space wavelength of 3.5 GHz) as shown in Fig. 6 (top). The current path of the resonant frequency point of 5.5 GHz mainly focuses on the right outer branch which can also contribute a 0.25-wavelength resonant mode (PA works for i0.25-wavelength monopole-like mode, the length of the current path is: $L_{\mathrm{GHIJ}} = 11.3$ mm $\approx 0.21\ \lambda_1$, λ_1 is the free

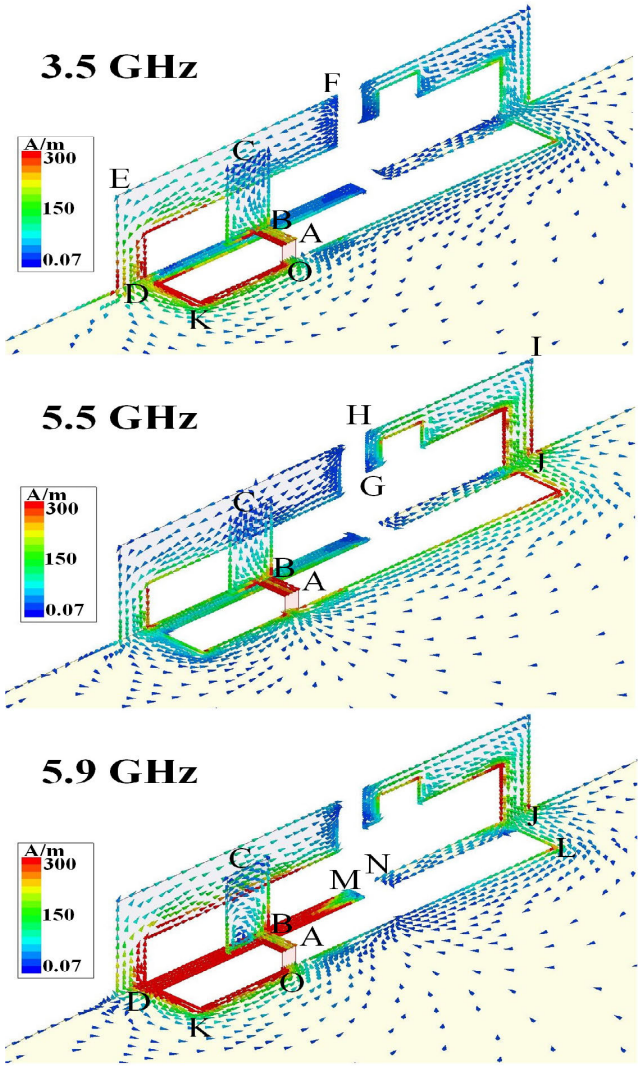

FIGURE 6. Simulated vector current distributions of the proposed antenna element and ground plane at different resonant frequency.

space wavelength of 5.5 GHz) as shown in Fig. 6 (middle). It can also be clearly seen from Fig. 6 (bottom) that the current path of 5.9 GHz is mainly focused on the slots on the ground plane, which is a typical 0.25-wavelength open-slot mode (OS works for 0.25-wavelength open-slot mode, the length of the current path is: $L_{\mathrm{MDKO}} = 12.5$ mm $\approx 0.25\ \lambda_2$, λ_2 is the free space wavelength of 5.9 GHz).

C. PARAMETER ANALYSIS

In the application of the 8 × 8 MIMO antenna system in the 5G mobile terminals, it would be good if the performance of antenna element does not vary much when the antenna element is moved for one position to another. This is because the possibility of adopting the same of at least very similar antenna structure at different positions can make the design procedure of MIMO antenna system easy and simple.

Here, we define the variable D as the distance from the leftmost edge of the antenna element to the short edge of the ground plane, that is, the position of the antenna element relative to the long edge of the ground plane as shown

in Fig. 7. And Fig. 8 illustrates how the reflection coefficient of the antenna element changes while the antenna element is moved from its original position (i.e. $D = 6$ mm) toward the center, along the long edge of the smartphone. As can be seen in Fig. 8, the 6-dB impedance bandwidths of the antenna element changes very little and can all cover the required triple-band of 3300-3800 MHz, 4800-5000 MHz and 5150-5925 MHz, even though the $|S_{11}|$ at few frequency points within 4800-5000 MHz of the higher band gets a little smaller but still more than 5.2 dB as the antenna element gets closer to the center of ground plane. Meanwhile, slight changes in the total efficiency of the antenna element relative to different locations can also indicate that the designed antenna element always works well during this shift as shown in Fig. 9. And these features studied above can also be used as guidance to arrange the eight MIMO antennas in the mobile terminal.

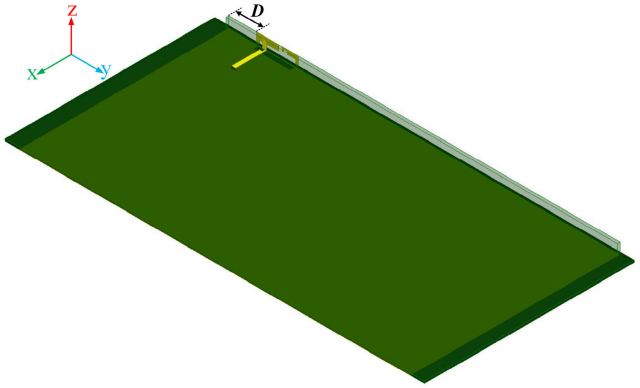

FIGURE 7. Location (*D*) of the proposed antenna element along the long edge of the ground plane.

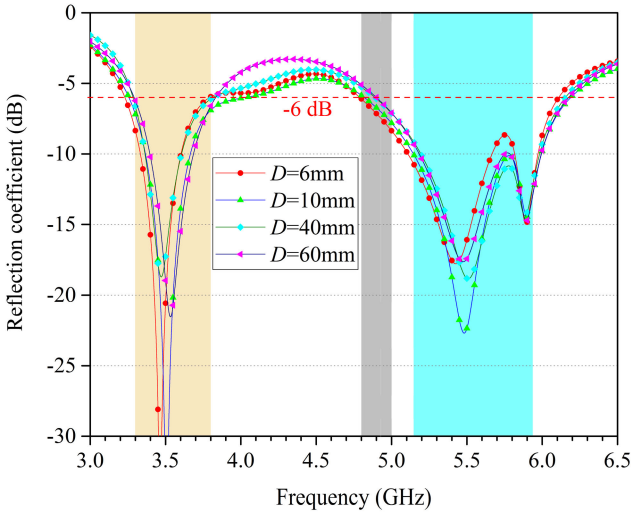

FIGURE 8. Simulated reflection coefficients of the proposed antenna element varies as a function of *D*.

D. PERFORMANCE OF THE 8 × 8 MIMO ANTENNA SYSTEM

Based on the characteristics of the antenna element analyzed and discussed above and the trade-off between bandwidth, isolation and total efficiency of the 8-antenna MIMO system,

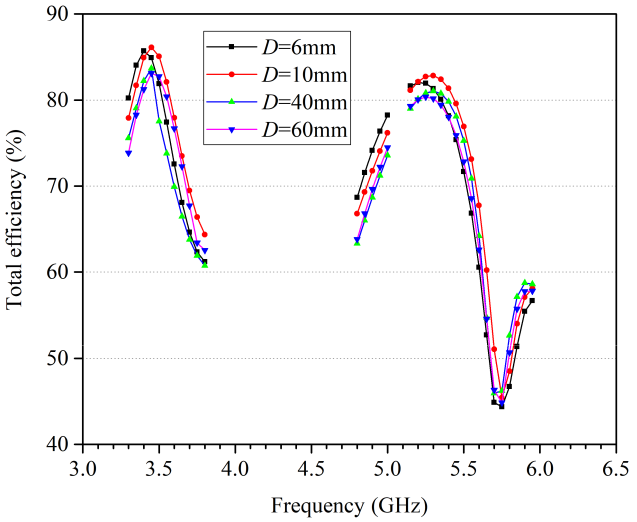

FIGURE 9. Simulated total efficiencies of the proposed antenna element varies as a function of *D*.

the final parameter results of the proposed eight-element antenna array shown in Fig. 1(a) are obtained, which are used to evaluate the performance of the final triple-band 8 × 8 MIMO antenna system in this design. In other words, we have also analyzed three other arrangements of the 8-antenna MIMO system based on the same antenna element to compare with the proposed final configuration of the 8-antenna MIMO system in the following.

To discuss the MIMO antenna performance, *S*-parameters of the proposed eight-element antenna array is first studied and the reflection coefficient therein is plotted in Fig.10 while the transmission coefficient therein is plotted in Fig. 11. It should be note that, because the proposed MIMO antenna system is absolutely symmetric, only the necessary parameter

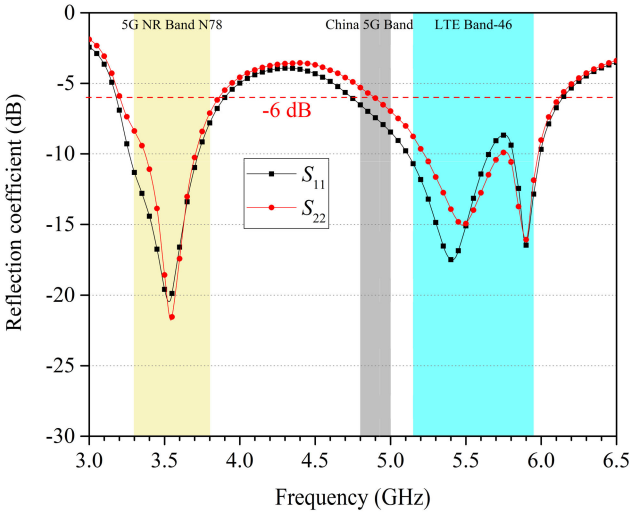

FIGURE 10. Simulated reflection coefficients of the proposed eight-element antenna array.

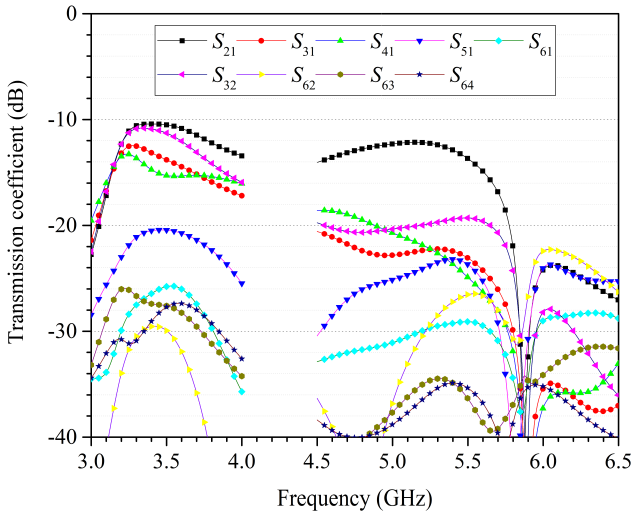

FIGURE 11. Simulated transmission coefficients of the proposed eight-element antenna array.

results have been presented and the same results have been omitted for the sake of brevity.

As shown in Fig. 10, it illustrates the simulated reflection coefficients (S_{ii}, $i = 1-8$) of the proposed 8-antenna MIMO system. Based on the architecture of the 8-antenna array shown in Fig. 1 (a), four antennas close to the four corners of the system substrate, namely, Ant. 1, Ant. 4, Ant. 5 and Ant. 8, exhibits an operating bandwidth is wider than that of the four antennas arranged inside along the long-edge of the ground plane of mobile terminal, namely, Ant. 2, Ant. 3, Ant. 6 and Ant. 7, as shown in Fig. 10. This result not only accords with the conclusion in Fig. 8, but also reflects that the coupling between antennas in the multi-antenna system will change the original resonant frequency point and bandwidth of the antenna element therein at different degrees. However, the operating bandwidth of the proposed 8-antenna MIMO system can cover triple-band of 3.3-3.8 GHz, 4.8-5 GHz and 5.15-5.925 GHz for reflection coefficient less than -6 dB (reflection coefficients of Ant. 2, 3, 6, 7 in the 4.8-5 GHz band are less than -5.3 dB).

In addition, the proposed eight-element antenna array still has an isolation degree of over 10.5 dB within the entire operating bands without introducing additional decoupling structures, as shown in Fig. 11, which indicates that the large distance (about 0.25 λ_0 or more, λ_0 is free space wavelength at 3.5 GHz) between the adjacent antenna elements makes the antenna array itself have a certain isolation effect. It can be seen from Fig. 11 that the isolations S_{51}, S_{61} and S_{62} are always better than 20.5 dB, 25.8 dB and 23 dB, respectively, which indicate that the proposed compact 8-antenna MIMO system can ensure great isolation between the two adjacent antennas respectively arranged on the two different 4-antenna linear sub-array shown in Fig. 1.

It can also be seen from Fig. 11 that the worst isolation occurs mainly on S_{21} in the lower operating band of 3300-3800 MHz, followed by S_{32}. So, in order to show the relation of mutual coupling with varying inter-element spacing, the results of S_{21} by changing with d12 (the spacing between Ant. 1 and Ant. 2 defined in Fig. 1(b)) can give more insights. Because of the symmetric arrangement, the geometrical parameters given in Fig. 1(b) have the following relations: d12 = d34, d12 + d23 + d34 + 4L + 2D = 140 mm. According to the size of the free space wavelength, we can establish a conversion relationship of d12 respect to λ_0 (λ_0 is the free space wavelength of 3.5 GHz), while the values of L and D are fixed (L = 15 mm, D = 6 mm). The corresponding results are plotted in Fig. 12(a). As can be seen from Fig. 12(a), the mutual coupling between two antenna elements changes with the spacing, and the smaller the spacing, the smaller the isolation. Furthermore, the mutual coupling can obviously affect the resonance characteristics and radiation efficiency of the 8-antenna MIMO system, that is, the stronger the mutual coupling, the more the resonant point shifts toward low frequency, and the lower the total efficiencies, the corresponding simulated results are shown in Fig. 12(b), (c), (d) and (e), respectively.

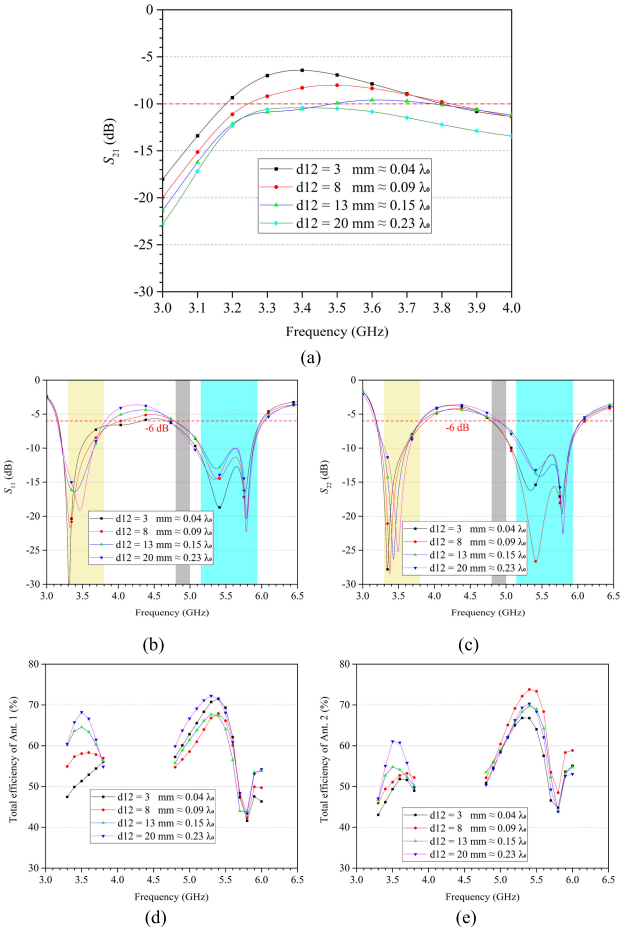

FIGURE 12. Simulated results of the proposed eight-element antenna array varies as a function of d12. (a) S_{21} in the lower band, (b) S_{11}, (c) S_{22}, (d) Total efficiency of Ant. 1, and (e) Total efficiency of Ant. 2.

Moreover, the simulated current distributions of the proposed antenna array at 3.5 GHz are presented in Fig. 13,

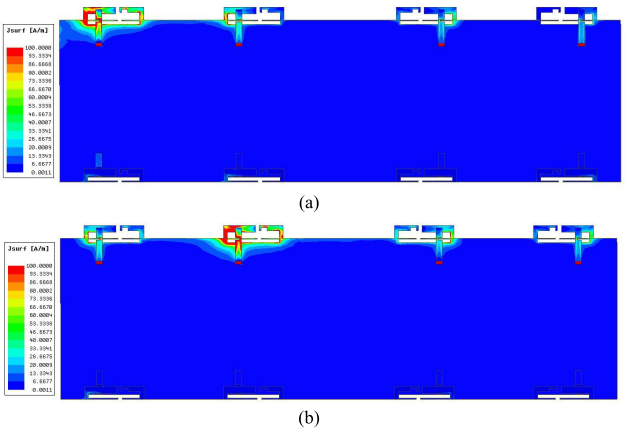

FIGURE 13. Simulated current distribution of the proposed eight-element antenna array at 3.5 GHz. (a) Ant. 1 is excited, and (b) Ant. 2 is excited, while all the other antennas are terminated to 50-ohm loads.

they provide a further understanding of the mutual coupling between antenna elements.

Certainly, the antenna array also has enough space to achieve a higher isolation if it is necessary to intentionally increase the degree of isolation in the future, using the simple decoupling structures proposed in the previous published literatures mentioned above, such as the neutralization line. However, in order to reduce the influence of other structures on the performance of the proposed 8-antenna array in mobile terminal, only the existing antenna element structure and array architecture are considered, and the realization of antenna miniaturization and multi-mode excitation is mainly discussed in this paper.

The corresponding simulated total radiation efficiencies of the proposed eight-element antenna array are 47%-68%, 51%-67% and 43%-73% within the triple-band of 3.3-3.8 GHz, 4.8-5 GHz and 5.15-5.925 GHz, respectively, as shown in Fig. 14. As expected, the total efficiencies of

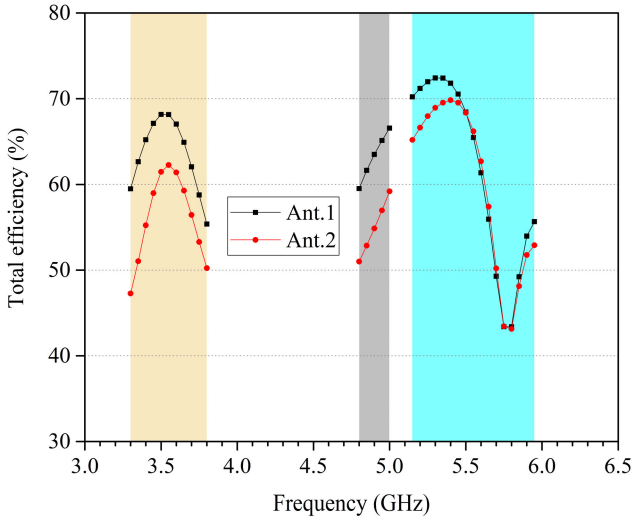

FIGURE 14. Simulated total efficiencies of the proposed eight-element antenna array.

the four antennas arranged in the middle of the long edge of the system ground are lower than the four antennas arranged close to the four corners of the system ground. There are two main reasons, using Ant. 2 (middle) and Ant. 1 (corner) as an example, one is the radiation efficiency is related with the antenna location, as explained in Fig. 9, the farther to the short side of the ground, the lower the efficiency. The second is that the coupling effect is different for these two antennas. Ant. 2 is coupled to both the left and right antennas, as shown in Fig. 13(b), while Ant. 1 is mainly coupled with adjacent Ant. 2, as shown in Fig. 13(a). As a result, the efficiency of Ant. 2 is lower than that of Ant1. Fortunately, all the antenna radiation efficiencies are still above 43%, and the maximum can be reached 73% within the entire required bands, which are acceptable for the 8-antenna MIMO system.

To compare the effects of different array element arrangements, Fig. 15 shows three referential arrangements of the eight-element antenna array and the proposed one based on the same parameters of L, d12, d23, d34, L_1, W and D. Here, we use the red arrow to indicate the 'orientation' of antenna element in the 8-antenna array. At the same time, the numbering sequence of antenna elements in these three cases is the same as the numbering sequence of antenna elements in Fig. 1(a). Since for all cases, the Ant. 5-8 are arranged exactly the same way as Ant. 1-4, we only describe the Ant. 1-4's orientations.

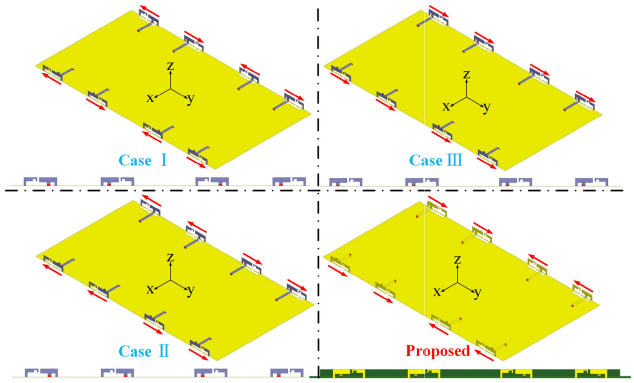

FIGURE 15. Three referential arrangements (Cases I, II and III) of the eight-element antenna arrays as compared with the proposed one.

As shown in Fig. 15, In Case I, Ant. 1-Ant. 4 are arranged in the alternative direction. In Case II, Ant. 1 and Ant. 2 are arranged in same sequence pointing to the left (−y axis) and Ant. 3 and Ant. 4 are arranged in the same sequence but pointing to the right (+y axis). In Case III, Ant. 1-Ant. 4 are arranged in the same sequence pointing to the right direction (+y axis).

In simulations, similarly, only the necessary parameter results have been presented and the same results have been omitted for the sake of brevity. Fig. 16(a) and Fig. 16(b) show the simulated antenna's S-parameters and total efficiencies for Case I, respectively. Because Ant. 1 and Ant. 2 therein interact with each other greatly, resulting in a deviation (about

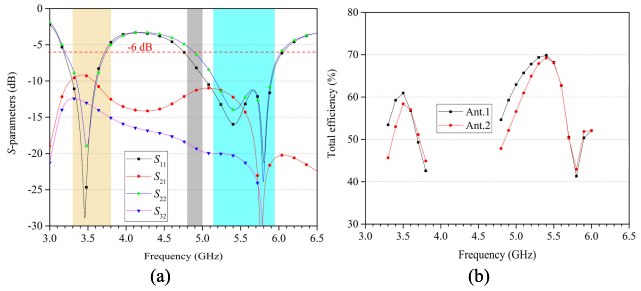

FIGURE 16. Simulated *S*-parameters and total efficiencies of the eight-element antenna array in Case I. (a) *S*-parameters, and (b) total efficiencies.

100 MHz) of their bandwidths in the lower operating band so that they cannot completely cover the required operation bands. Moreover, the mutual coupling between antenna elements in the lower frequency band is also relatively strong which resulting in a relatively low isolation with the minimum value of only 8.5 dB. At the same time, the total efficiencies of the antennas in Case I are only 42%-61% in the lower operating band which are also deteriorated due to the relatively strong degree of coupling, as shown in Fig. 16(b). From the results in Case I, it can also be concluded that the direct adjacent of the feeding ports of the antenna elements causes an increase in the degree of coupling between the antenna elements, thereby affecting the performance indicators of the MIMO antennas as expected.

The coupling is most prominent in the ground current coupling, this is because that according to the working principle of the antenna element analyzed above (subsection B), each resonant frequency point should be generated in cooperation with the ground, so that the current distribution of each excitation mode of the antenna element on the ground is relatively large. The same results also occurred in Case II, that is, the bandwidths of the antennas have a deviation in the lower operating band, and S_{32} becomes worse while S_{21} becomes better, and the total efficiency of Ant. 1 becomes better while that of Ant. 2 becomes worse due to the similar arrangement, and the corresponding simulated results are shown in Fig. 17(a) and Fig. 17(b), respectively.

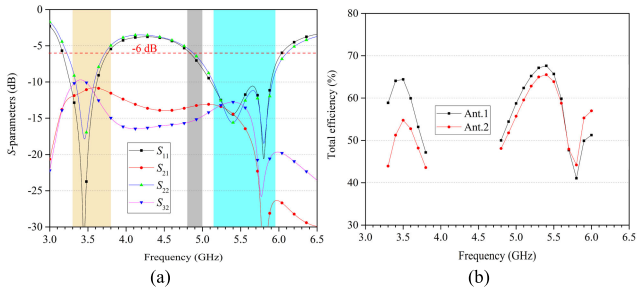

FIGURE 17. Simulated *S*-parameters and total efficiencies of the eight-element antenna array in Case II. (a) *S*-parameters, and (b) total efficiencies.

For the Case III, the isolations in the full operating bands are improved due to the indirect adjacent arrangement of the feeding ports. However, because of the asymmetric arrangement of the antennas on the linear sub-array, their operating bandwidths are also shifted so that they cannot fully cover the required triple-band, as shown in Fig. 18(a). Meanwhile, the total radiation efficiencies in this case has increased as expected. However, there are also some frequencies with low total efficiencies in the lower operating band, especially in the band of 3.7-3.8 GHz, as shown in Fig. 18(b), which still needs to be improved.

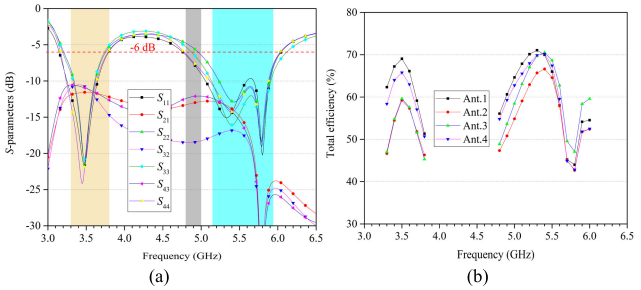

FIGURE 18. Simulated *S*-parameters and total efficiencies of the eight-element antenna array in Case III. (a) *S*-parameters, and (b) total efficiencies.

For the case of proposed one, the feeding ports of the antenna elements are all indirect adjacent to each other. And, from the simulated results analyzed in Fig. 10, 11 and 14, one can see that the isolations between the antenna elements are greater than 10.5 dB in the lower operating band and greater than 12 dB in the higher operating bands while the required bandwidths and better total efficiencies are also obtained. Therefore, from the all results above, the finally proposed arrangement of the eight-element antenna array has relatively good comprehensive performance for being used in practical applications.

E. EFFECTS OF USER'S HANDS

The effects of user's hand(s) for the proposed 8 × 8 MIMO antenna system is investigated in this paper. Fig. 19(a) and Fig. 19(b) gives the typical single-hand hold (SHH) and dual-hand hold (DHH) scenario of the user's hand, respectively. The proposed 8-antenna array at triple-band of 3.3-3.8 GHz, 4.8-5 GHz and 5.15-5.925 GHz normally operate at data mode, so the effect of a user's head is not considered. The corresponding simulated results within these two hold scenarios are shown in Fig. 20-22. For each hand hold scenario, three identical parameters, namely, reflection coefficient (bandwidth), transmission coefficient (isolation) and total radiation efficiency, are analyzed and presented.

For SHH mode, the simulated *S*-parameters and total efficiencies are shown in Fig. 20(a), Fig. 21(a) and Fig. 22(a), respectively. From the data in Fig. 20(a), the reflection coefficients of the eight-antenna array are influenced at different degrees, especially the results of the antennas 1, 2, 3, 5 and 6 located at the holding positions. This is because the SHH mode is equivalent to introducing asymmetric loss medium around the antennas, so that much EM (electromagnetic)

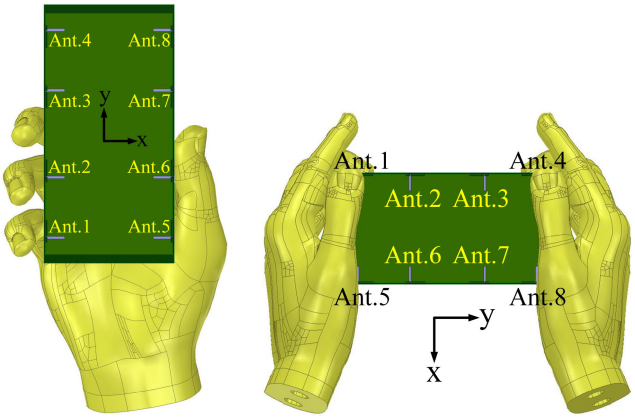

FIGURE 19. Two typical hand-hold scenarios for mobile terminals. (a) Single-hand hold, (b) dual-hand hold.

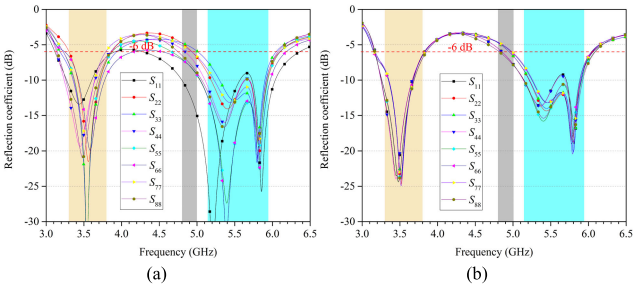

FIGURE 20. Simulated reflection coefficients of the proposed eight-element antenna array with (a) single-hand and (b) dual-hand.

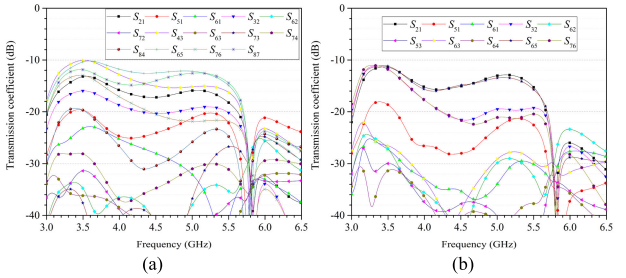

FIGURE 21. Simulated transmission coefficients of the proposed eight-element antenna array with (a) single-hand and (b) dual-band.

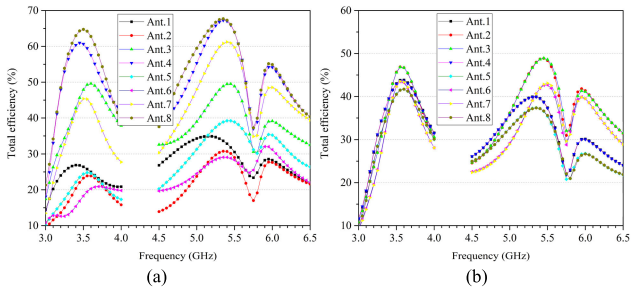

FIGURE 22. Simulated total efficiencies of the proposed eight-element antenna array with: (a) single-hand and (b) dual-band.

energy has been absorbed by the antennas who close to the fingers, which also resulting in the isolations between the specific antennas above becomes better, as also can be seen in Fig. 21(a). Compared to the free space case, the antenna total radiation efficiencies drop for the with hand case. However, the total efficiencies of the 8 antennas are all more than 13% within the entire operating band are still acceptable for practical scenario, as shown in Fig. 22(a). In particular, the antenna with the most phantom hand coverage suffers bigger efficiency degradation, as expected.

For DHH mode, the simulated S-parameters and total efficiencies are shown in Fig. 20(b), Fig. 21(b) and Fig. 22(b), respectively. From the data in Fig. 20(b), the reflection coefficients of the eight-antenna array are influenced at the same degrees owing to the symmetrical DHH mode and have little deterioration. In which, the reflection coefficients of the 8 antennas in the band of 4.8-5 GHz are degraded, especially for the four antennas located inside, but they are all less than −4.8 dB with good isolations and good total efficiencies.

In general, the reflection coefficients are considered to be that the 8-antenna array can still cover the triple-band of interest with DHH mode which are also acceptable for practical applications. Due to the symmetrical of the DHH mode, the isolations between any two antenna elements becomes better than that in the free space case owing to the absorption of the EM energy, as shown in Fig. 21(b). As shown in Fig. 22(b), the total efficiencies decrease due to the absorption effect of the hands. However, the worst antenna total radiation efficiency is still better than 22%, which is still acceptable for practical scenario.

SAR (Specific Absorption Rate) is a measure of the rate at which the energy is absorbed by the human body when exposed to a radio frequency (RF) electromagnetic field. It is defined as the power absorbed by per mass of tissue and has units of watts per kilogram (W/kg). As shown in Fig. 23, to verify the antenna radiation to human hands, the SAR simulation models (SHH mode and DHH mode) are studied and performed based on the FCC standard. In simulations, the total input power of all 8 antennas together is 100 mW or 20 dBm, and the total SAR reported is calculated by the sum of each element's SAR when they are excited at the same time with the evenly divided power from the total 100 mW, as 11 dBm. The simulated maximum value of SAR for single-hand hold (SHH) mode and each hand of dual-hand hold (DHH) mode is 1.459 W/Kg and 0.66 W/Kg, respectively. The simulated average SAR values at different resonant frequencies are under the SAR limit of 1.6 W/kg for 1-g tissue, which are acceptable for practical mobile applications.

IV. EXPERIMENTAL RESULTS AND DISCUSSION

As shown in Fig. 24, based on the simulated results of the proposed eight-element triple-band antenna array analyzed and discussed above, the prototype has been manufactured and used to measure the corresponding parameter results. All the parameter results of the proposed antenna array are measured under the circumstance that one antenna element is excited while all the other elements are connected to 50-ohm matched loads in the microwave anechoic chamber and with the VNA.

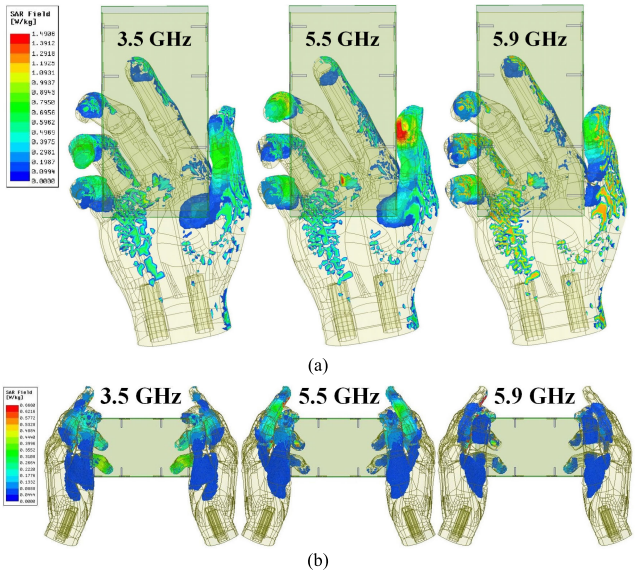

FIGURE 23. Simulated distributions of SAR in hand(s) at different resonance frequency. (a) single-hand, and (b) dual-band.

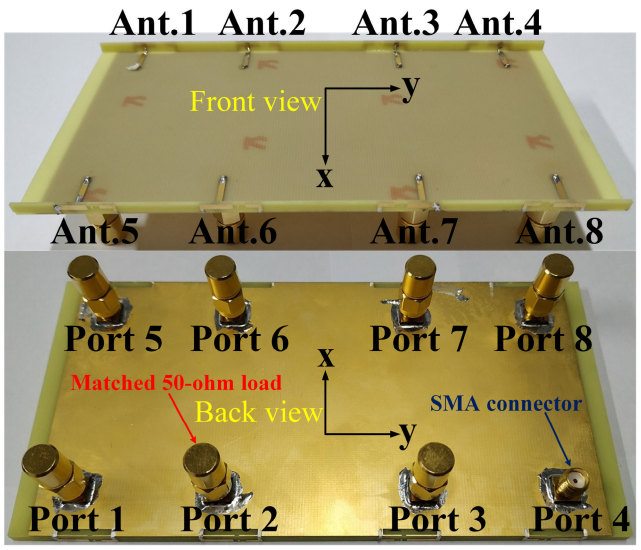

FIGURE 24. Fabricated prototype of the proposed compact triple-band eight-element antenna array.

A. MEASURED RESULTS OF S-PARAMETERS, TOTAL EFFICIENCY AND 2D RADIATION PATTERNS

The measured *S*-parameter results are shown in Fig. 25 and Fig. 26. Due to the fabrication tolerance, SMA welding issues and rough handmade effects, the resonance frequencies and bandwidths of each antenna element in the proposed array has been deviated or changed a little. Overall, the reflection coefficient curves in Fig. 25 shows that the proposed 8-antenna MIMO system can operate in triple-band of 3300-3800 MHz, 4800-5000 MHz and i5150-5925 MHz with $|S_{11}|$ >6 dB, and the transmission coefficient curves in Fig. 26 shows that the isolations between any two antenna

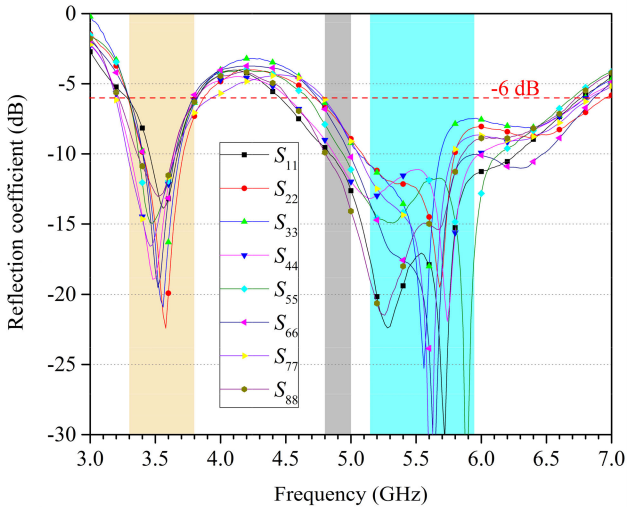

FIGURE 25. Measured reflection coefficients of the proposed compact triple-band eight-element antenna array.

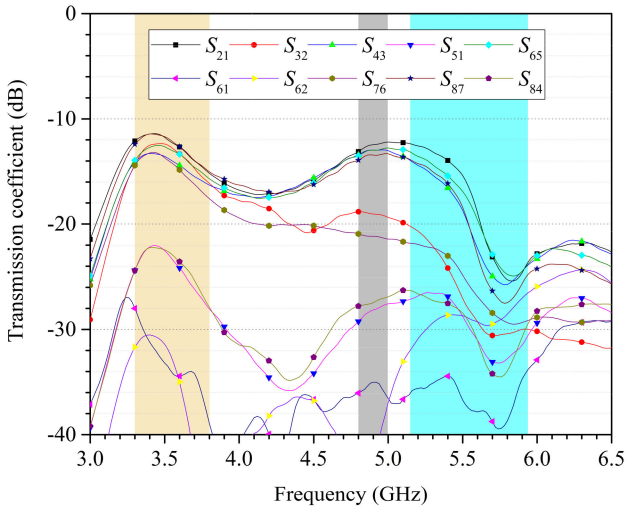

FIGURE 26. Measured transmission coefficients of the proposed compact triple-band eight-element antenna array.

elements are all more than 11.5 dB within the desired operating bands.

Compared with the simulated results, the bandwidths of Ant. 2, 3, 6, 7 becomes slightly better within the China 5G band of 4800-5000 MHz, and all isolation values are 1 dB better. As shown in Fig. 27, within the entire desired operating bands, the measured antenna total efficiencies are all better than 42% but less than 76% which is basically consistent with the simulated results and promising for the 8 × 8 MIMO system. Generally speaking, the measurements and the simulations agree quite well, though sometimes the actual losses are higher than expected, but still acceptable.

The realized peak gains of the Ant. 1, Ant. 2, Ant. 6 and Ant. 8 are presented in Fig. 28, which are between 2.0 dBi to 3.6 dBi for the operating band of 3.3-3.8 GHz and 2.1 dBi to 4.8 dBi for the operating band of 4.8-5.925 GHz. The measured radiation patterns in the xoy and yoz planes of the

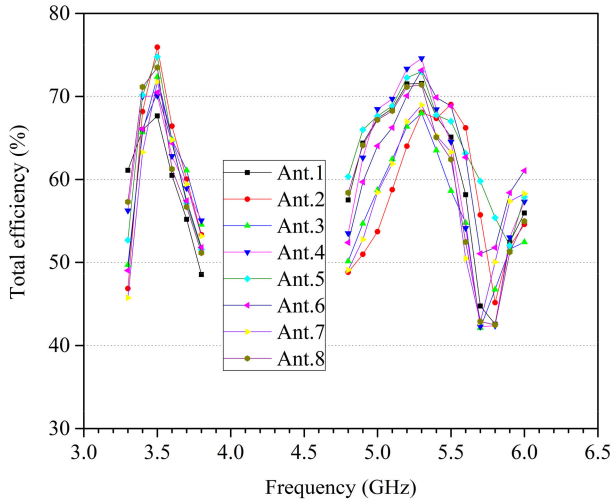

FIGURE 27. Measured total efficiencies of the proposed compact triple-band eight-element antenna array.

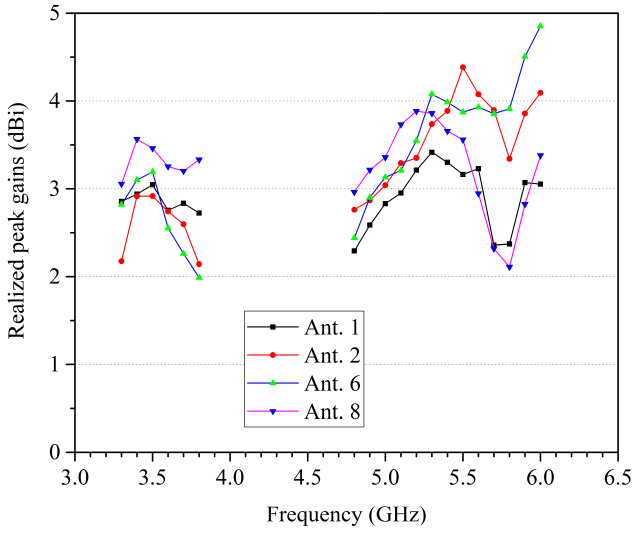

FIGURE 28. Measured realized peak gains of the Ant. 1, 2, 6, 8.

Ant. 1, Ant. 2, Ant. 6 and Ant. 8 in the proposed 8-antenna MIMO system at 3500 MHz, 5500 MHz and 5900 MHz are shown in Fig. 29 and Fig. 30, respectively. Here, Ant. 1 and Ant. 2 are used to represent the adjacent nearest antenna combination, while Ant. 6 and Ant. 8 are used to represent the indirect adjacent antenna combination in the proposed eight-antenna array, and the two combinations are located in two different linear subarrays, respectively. Finally, their results are used to characterize the radiation performances of the whole eight-element antenna array. One can see from Fig. 29 and Fig. 30 that each antenna has its own unique radiation pattern, different from those of other antennas, with omnidirectional radiation characteristics; and the maximum gains of each antenna element pointing to different directions at a certain frequency point. At the same time, it is easy to see from these two figures that the patterns of the two

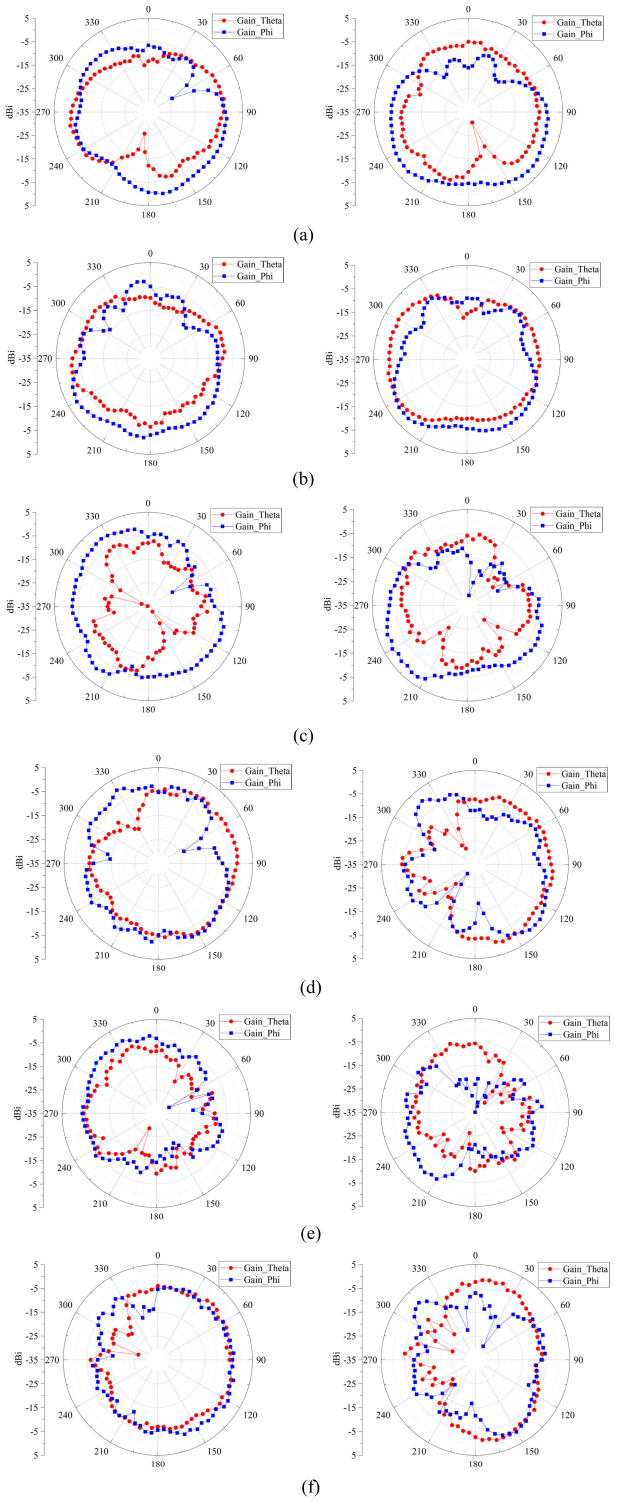

FIGURE 29. Measured 2D radiation patterns of Ant. 1 (left column) and Ant. 2 (right column) of the proposed compact triple-band 8 × 8 MIMO antenna system at (a) 3.5 GHz, xoy plane. (b) 3.5 GHz, yoz plane. (c) 5.5 GHz, xoy plane. (d) 5.5 GHz, yoz plane. (e) 5.9 GHz, xoy plane. (f) 5.9 GHz, yoz plane.

indirect adjacent antennas have distinctly different directions, in which, although the patterns of the two direct adjacent antennas have different directions, their difference in pointing is smaller than that of the two indirect adjacent antennas.

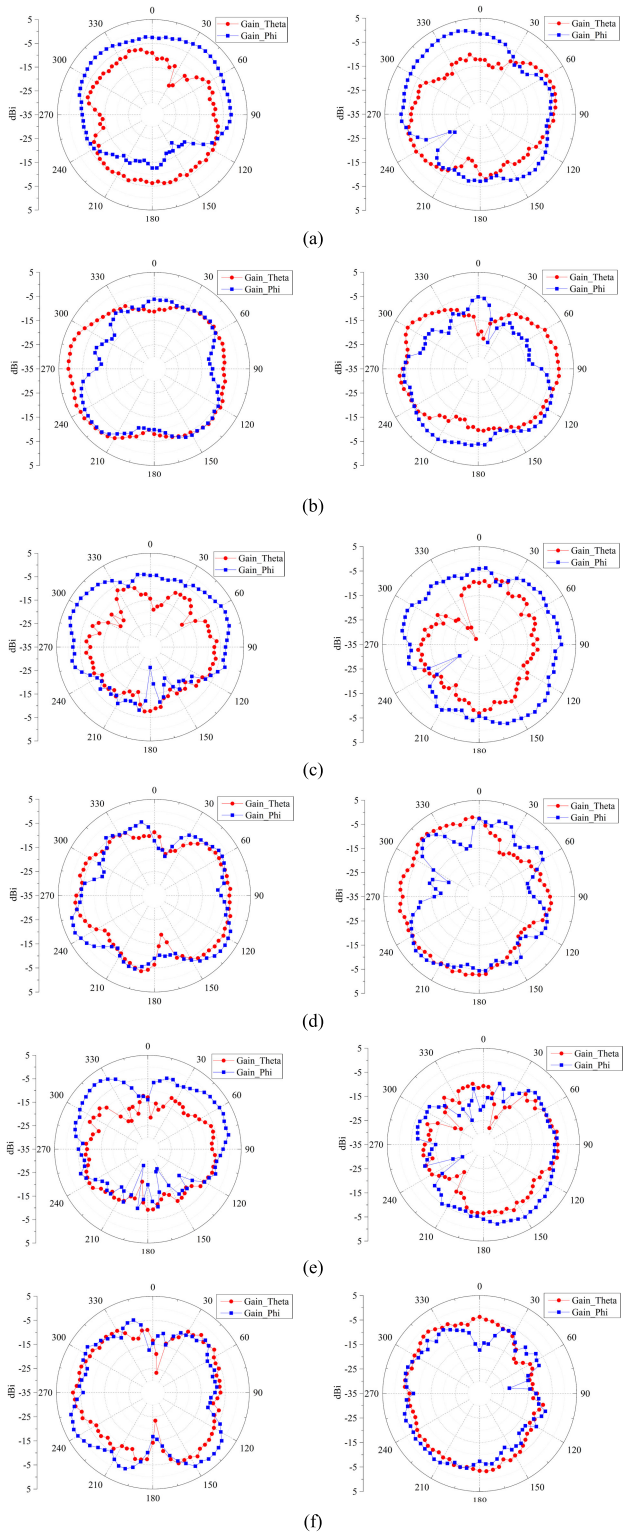

FIGURE 30. Measured 2D radiation patterns of Ant. 6 (left column) and Ant. 8 (right column) of the proposed compact triple-band 8 × 8 MIMO antenna system at (a) 3.5 GHz, xoy plane. (b) 3.5 GHz, yoz plane. (c) 5.5 GHz, xoy plane. (d) 5.5 GHz, yoz plane. (e) 5.9 GHz, xoy plane. (f) 5.9 GHz, yoz plane.

However, the radiation patterns of the 8 antennas with different pointing directions to each other combined with high port isolations should make a great contribution to achieve smaller value of ECC for any two antenna elements, and thereby an enhanced channel capacity (CC) for the MIMO operation can be obtained, which will be presented in the next subsection.

B. MIMO PERFORMANCE

In this subsection, in addition to the measured results of bandwidth, total efficiency and far field patterns, there are two important indicators used to evaluate the performance of the 8-antenna triple-band MIMO system: ECC (Envelope Correlation Coefficient) and CC (Channel Capacity).

Firstly, the ECC defines the correlation level between the radiation patterns of any two antenna elements in a multi-antennas array. It is the most important indicator to judge the performance such as diversity gain of a MIMO system. When the correlation is high, the MIMO performance will deteriorate, especially when the envelope correlation exceeds 0.5. This is because MIMO systems rely on the independence among the received signals to provide diversity and/or independent channels in spatial multiplexing. The complex correlation coefficient between antenna element i and antenna element j, based on the far field patterns, is expressed as:

$$\rho_{ij} = \frac{\int_0^{2\pi}\int_0^{\pi} A_{ij}(\theta,\varphi)\sin\theta d\theta d\varphi}{\sqrt{\int_0^{2\pi}\int_0^{\pi} A_{ii}(\theta,\varphi)\sin\theta d\theta d\varphi \int_0^{2\pi}\int_0^{\pi} A_{jj}(\theta,\varphi)\sin\theta d\theta d\varphi}} \tag{1}$$

where

$$A_{ij}(\theta,\varphi) = E_{\theta,i}(\theta,\varphi)E^*_{\theta,j}(\theta,\varphi) + E_{\varphi,i}(\theta,\varphi)E^*_{\varphi,j}(\theta,\varphi) \tag{2}$$

The $E_\theta/\varphi, i/j(\theta, \varphi)$ in formula (2) is the θ (or φ)-polarized electric far-field pattern of the antenna i (or j) in spherical coordinates. And the simulated and measured complex radiation far field of the antennas can be obtained from either CST and 3D measurement in a microwave anechoic chamber. The ECC can also be estimated from the S-parameters using the formula as following:

$$\rho_{ij} = \frac{\left|S^*_{ii}S_{ij} + S^*_{ji}S_{jj}\right|^2}{\left(1-\left(|S_{ii}|^2+|S_{ji}|^2\right)\right)\left(1-\left(|S_{jj}|^2+|S_{ij}|^2\right)\right)} \tag{3}$$

However, the accuracy of the method relies heavily on the assumption of 100 % radiation efficiency, and significant error can occur even for relatively high radiation efficiencies. In this study, the calculated ECCs from the measured complex far field patterns of the proposed 8-antenna MIMO system are obtained by using the formulae (1) and (2) are plotted in Fig. 31. It can be obviously observed from Fig. 31 that the ECC values are less than 0.12 in which the minimum value is even 0.001 which are all much lower than the typic carrier's requirement of 0.5, over their corresponding desired bands of interest.

TABLE 1. Performance comparison between the proposed eight-element antenna array and referential works.

Ref.	Operating Bandwidth (MHz)	Isolation (dB)	Total Efficiency (%)	ECC	Peak Channel Capacity (bps/Hz)	Applications	Metal Frame	Matching Circuit	Occupied Area[a] (mm×mm)
[30]	3400-3600	> 10	40-60	< 0.1	36 (8×8 MIMO)	Cellular	No	Without	150×1[b] 10×6.2[c]
[22]	2550-2650	> 12.5	55-63	< 0.15	40 (8×8 MIMO)	Cellular	No	Without	17.8×4 31.2×5
[20]	3400-3600	> 19.6	60-70	< 0.01	36 (8×8 MIMO)	Cellular	No	Without	N/A[d] 17.4×6
[23]	3400-3600	> 17	49-73	< 0.07	Not given	Cellular	No	Without	150×1[b] 12×7[c]
[36]	3400-3800	> 10	42-62	< 0.1	47 (10×10 MIMO)	Cellular	No	Without	8×3 N/A[d]
[21]	3400-3600	>17	58-74	< 0.1	19 (4×4 MIMO)	Cellular	No	Without	150×1[b] 20×6.2[c]
[37]	3400-3600	> 10	40-60	< 0.32	70 (16×16 MIMO)	Cellular	No	Without	8×3 N/A[d]
[35]	3400-3600	> 10	56-70	< 0.2	40 (8×8 MIMO)	Cellular	No	Without	16.7×3 N/A[d]
[17]	3400-3600	>12.5	50-70	< 0.02	34.25 (8×8 MIMO)	Cellular	No	Without	17×17[c] 17×6
[18]	2400-3600	> 15	50-60	< 0.2	57 (12×12 MIMO)	Cellular	No	Without	15×3 30×4.4
[19]	3400-3600	> 17.5	62-76	< 0.05	40.8 (8×8 MIMO)	Cellular	No	Without	21.5×3 N/A[d]
[38]	2550-2650	> 13	48-58	< 0.2	39 (8 × 8 MIMO)	Cellular	No	Without	18.6×18.6 N/A[d]
[34]	3400-3600	> 10	55-59	Not given	1.2 bit/(s Hz)	Cellular	No	With	16×5 5×5
[39]	3300-6000	> 11	40-71	< 0.12	40 (8 × 8 MIMO)	Cellular	Yes	Without	15×3 15×6
[26]	3400-3600 4800-5000	> 17.5	55-68 51-78	< 0.14	18 (4×4 MIMO)	Cellular	No	Without	150×1[b] 22×6.8[c]
[33]	3400-3600 5150-5925	> 11.2	51-59 62-80	< 0.1	40.9 (8×8 MIMO)	Cellular	No	Without	16.3×10 N/A[d]
[27]	3400-3600 4800-5100	> 11.5	41-72 40-85	< 0.08	38.5 (8×8 MIMO)	Cellular	No	Without	150×1[b] 15×6.2[c]
[32]	1880-1920 2300-2620	> 10	40-55 50-70	< 0.1	Not given	Cellular	No	Without	16×15 N/A[d]
[28]	2496-2690 4800-5100	> 10	Not given	< 0.2	Not given	Cellular	No	Without	17×6[c] 17×5
[40]	3000-11000	> 15	Not given	< 0.5	Not given	Others	No	Without	25×15 N/A[d]
[41]	3100-10600	> 15	Not given	< 0.2	Not given	Others	No	Without	29×25 N/A[d]
[42]	3000-15000	> 20	Not given	< 0.5	Not given	Others	No	Without	18×18 N/A[d]
[43]	4000-10000	> 15	Not given	< 0.03	Not given	Others	No	Without	23.8×12 N/A[d]
This work	3300-3800 4800-5000 5150-5925	> 10.5	55-72 50-65 43-73	< 0.12	37.6 (8 × 8 MIMO)	Cellular	No	Without	13×2 15×3

[a]Occupied area on the horizontal (ground clearance) and vertical planes of the mobile terminal, respectively, which are used to realize structural designs of the antenna element or the antenna array.
[b]The necessary clearance area between ground plane and frame for realizing antenna design.
[c]Two-antenna building block or antenna pairs printed on two long side-edges of the frame or antenna element placed on the system circuit board.
[d]No antenna body printed on two long side-edges of the frame or no clearance on ground plane.

Secondly, the CC (channel capacity) that is used to evaluate the performance of MIMO system can be expressed as following:

$$C = E\left\{\log_2\left[\det\left(I_N + \frac{SNR}{N}\right)HH^T\right]\right\} \quad (4)$$

where C is the channel capacity (CC), E denotes the expectation with respect to different channel realizations, SNR is the mean signal-to-noise ratio at the receiving side, N is the number of the antenna elements in a MIMO system, I_N denotes an identity matrix, H is the matrix of the channel

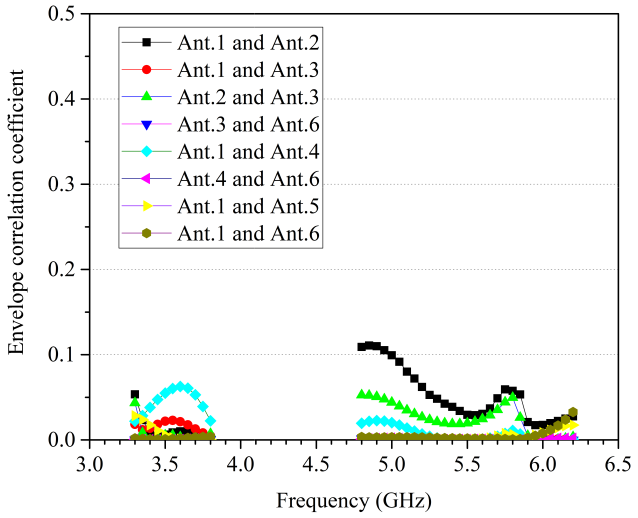

FIGURE 31. Calculated ECC of the proposed compact triple-band 8 × 8 MIMO antenna system.

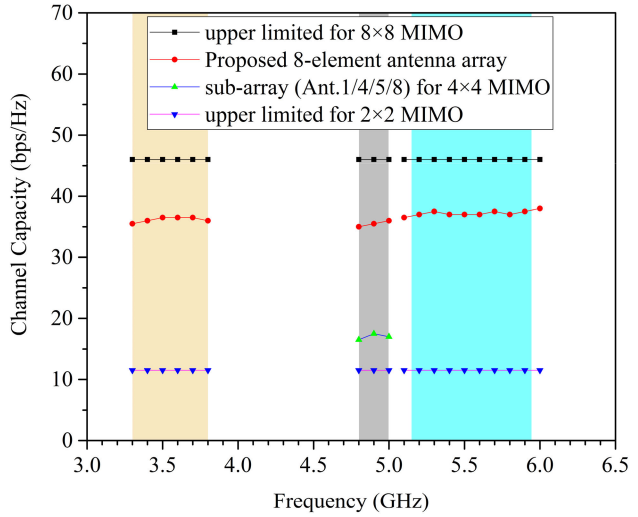

FIGURE 32. Calculated CC (channel capacity) of the proposed compact triple-band 8 × 8 MIMO antenna system.

capacity and $(.)^T$ denotes the Hermitian transpose. In this study, the achievable channel capacity for the 8 antennas as the receiver in the proposed triple-band 8 × 8 MIMO system with Rayleigh multipath environment and 20-dB signal-to-noise (SNR) is also computed and presented. Fig. 32 shows the obtained channel capacity of the proposed 8-antenna MIMO system in the 3 operating bands. The channel capacity in the N78, China 5G Band and LTE band-46 are respectively about 35.2-36.8, 34.9-37 and 35.5-37.6 bps/Hz.

Therefore, the calculated results of ECC and CC indicate that the 8 fabricated antennas operating in triple-band are promising to achieve good MIMO performances for mobile communication in the 5G mobile terminals.

Furthermore, in order to show the superiority of the proposed 8-antenna triple-band MIMO system, we have compared previous reported MIMO antennas and this work mainly in terms of bandwidth, isolation, total efficiency, ECC, peak Channel Capacity, applications, metal frame, matching circuit and occupied area, as shown in Table 1.

In Table 1, the first nineteen papers are designed for cellular applications while the last four papers are designed for other wireless terminal applications, we can compare our design with them separately. The main contribution of our work is that we proposed a triple-band and smaller size solution with comparable antenna element and MIMO performance with first nineteen papers, this is realized with new antenna design concept, implementation and system integration. For other wireless terminal application related papers (last four papers), they have wider bandwidth and better isolation but bigger antenna size in general than our work, this could partially because of the PCB terminal size and antenna location options are quite different from cellular device. That is to say, the proposed eight-element antenna array has the advantage of comprehensive performance, so that it can be well applied in the future multi-band ultra-thin 5G mobile terminals.

V. CONCLUSION

In this paper, we introduce an 8 × 8 MIMO antenna array based on a compact element consisting of the coupled-fed and parasitic arm with additional open-slot structure on the ground for triple-band (3300-3800 MHz, 4800-5000 MHz and 5150-5925 MHz) operation. The proposed antenna element or array can all obtain favorable working performance such as good measured effective 6-dB impedance bandwidth, good total efficiency (simulated results are from 43% to 73% while measured results are from 42% to 76% within the entire operating bands), good ECC (calculated results are all less than 0.12 in desired operating bands) and accepted isolation (simulated results are all more than 10.5 dB while measured results are all more than 11.5 dB within the entire operating bands) between antenna elements with advantages of small dimensions and simple structure for fabrication. The calculated channel capacity of the proposed 8 × 8 MIMO antenna system is 34.9-37.6 bps/Hz within the entire operating bands. The proposed eight-element antenna array could be one of the good candidates will be employed in the future ultra-thin 5G mobile terminals with narrow-frame, wide-screen and triple-band operation.

REFERENCES

[1] *5G Devices: What is 5G*. Accessed: Jun. 2017. [Online]. Available: https://www.4gltemall.com/5g.html

[2] WRC-15 Press Release. (Nov. 27, 2015). *World Radiocommunication Conference Allocates Spectrum for Future Innovation*. [Online]. Available: http://www.itu.int/net/pressoffice/press_releases/2015/56.aspx

[3] Asia Times. (Nov. 16, 2017). *China Reserves Spectrum for 5G Services*. [Online]. Available: http://www.atimes.com/article/china-reserves-spectrum-5g-services/

[4] *5G in the Sub-6 GHz Spectrum Bands*. [Online]. Available: http://www.rcrwireless.com/20160815/fundamentals/5g-sub-6ghz-tag31-tag99

[5] *5G NR (New Radio)*. Accessed: Dec. 12, 2018. [Online]. Available: http://3gpp.org/

[6] *Making the Best Use of Licensed and Unlicensed Spectrum*. Accessed: Sep. 2015. [Online]. Available: https://www.qualcomm.com/
[7] M. Zheng, H. Wang, and Y. Hao, "Internal hexa-band folded monopole/dipole/loop antenna with four resonances for mobile device," *IEEE Trans. Antennas Propag.*, vol. 60, no. 6, pp. 2880–2885, Jun. 2012.
[8] V. Plicanic, B. K. Lau, A. Derneryd, and Z. Ying, "Actual diversity performance of a multiband diversity antenna with hand and head effects," *IEEE Trans. Antennas Propag.*, vol. 57, no. 5, pp. 1547–1556, May 2009.
[9] Y. Li, Z. Zhang, J. Zheng, Z. Feng, and M. F. Iskander, "A compact hepta-band loop-inverted f reconfigurable antenna for mobile phone," *IEEE Trans. Antennas Propag.*, vol. 60, no. 1, pp. 389–392, Jan. 2012.
[10] K.-L. Wong, T.-W. Kang, and M.-F. Tu, "Internal mobile phone antenna array for LTE/WWAN and LTE MIMO operations," *Microw. Opt. Technol. Lett.*, vol. 53, no. 7, pp. 1569–1573, Jul. 2011.
[11] Y. Li, Z. Zhang, J. Zheng, and Z. Feng, "Compact heptaband reconfigurable loop antenna for mobile handset," *IEEE Antennas Wireless Propag. Lett.*, vol. 10, pp. 1162–1165, 2011.
[12] Y. Liu, Y. Luo, and S. Gong, "An antenna with a stair-like ground branch for Octa-band narrow-frame mobile phone," *IEEE Antennas Wireless Propag. Lett.*, vol. 17, no. 8, pp. 1542–1546, Aug. 2018.
[13] H. Xu, H. Wang, S. Gao, H. Zhou, Y. Huang, Q. Xu, and Y. Cheng, "A compact and low-profile loop antenna with six resonant modes for LTE smartphone," *IEEE Trans. Antennas Propag.*, vol. 64, no. 9, pp. 3743–3751, Sep. 2016.
[14] D. Wu, S. W. Cheung, and T. I. Yuk, "A compact and low-profile loop antenna with multiband operation for ultra-thin smartphones," *IEEE Trans. Antennas Propag.*, vol. 63, no. 6, pp. 2745–2750, Jun. 2015.
[15] Y.-L. Ban, J.-H. Chen, S. Yang, J. L.-W. Li, and Y.-J. Wu, "Low-profile printed Octa-band lte/wwan mobile phone antenna using embedded parallel resonant structure," *IEEE Trans. Antennas Propag.*, vol. 61, no. 7, pp. 3889–3894, Jul. 2013.
[16] C. Deng, Y. Li, Z. Zhang, and Z. Feng, "Planar printed multi-resonant antenna for Octa-band WWAN/LTE Mobile Handset," *IEEE Antennas Wireless Propag. Lett.*, vol. 14, pp. 1734–1737, 2015.
[17] M. Abdullah, S. H. Kiani, and A. Iqbal, "Eight element multiple-input multiple-output (MIMO) antenna for 5G mobile applications," *IEEE Access*, vol. 7, pp. 134488–134495, 2019.
[18] M.-Y. Li, Y.-L. Ban, Z.-Q. Xu, J. Guo, and Z.-F. Yu, "Tri-polarized 12-antenna MIMO array for future 5G smartphone applications," *IEEE Access*, vol. 6, pp. 6160–6170, 2018.
[19] Y. Li, C.-Y.-D. Sim, Y. Luo, and G. Yang, "High-isolation 3.5 GHz eight-antenna MIMO array using balanced open-slot antenna element for 5G smartphones," *IEEE Trans. Antennas Propag.*, vol. 67, no. 6, pp. 3820–3830, Jun. 2019.
[20] A. Zhao and Z. Ren, "Size reduction of self-isolated MIMO antenna system for 5G mobile phone applications," *IEEE Antennas Wireless Propag. Lett.*, vol. 18, no. 1, pp. 152–156, Jan. 2019.
[21] Z. Ren, A. Zhao, and S. Wu, "MIMO antenna with compact decoupled antenna pairs for 5G mobile terminals," *IEEE Antennas Wireless Propag. Lett.*, vol. 18, no. 7, pp. 1367–1371, Jul. 2019.
[22] M.-Y. Li, Y.-L. Ban, Z.-Q. Xu, G. Wu, C.-Y.-D. Sim, K. Kang, and Z.-F. Yu, "Eight-port orthogonally dual-polarized antenna array for 5G smartphone applications," *IEEE Trans. Antennas Propag.*, vol. 64, no. 9, pp. 3820–3830, Sep. 2016.
[23] L. Sun, H. Feng, Y. Li, and Z. Zhang, "Compact 5G MIMO mobile phone antennas with tightly arranged orthogonal-mode pairs," *IEEE Trans. Antennas Propag.*, vol. 66, no. 11, pp. 6364–6369, Nov. 2018.
[24] H. Xu, H. Zhou, S. Gao, H. Wang, and Y. Cheng, "Multimode decoupling technique with independent tuning characteristic for mobile terminals," *IEEE Trans. Antennas Propag.*, vol. 65, no. 12, pp. 6739–6751, Dec. 2017.
[25] W. Jiang, B. Liu, Y. Cui, and W. Hu, "High-isolation eight-element MIMO array for 5G smartphone applications," *IEEE Access*, vol. 7, pp. 34104–34112, 2019.
[26] Z. Ren and A. Zhao, "Dual-band MIMO antenna with compact self-decoupled antenna pairs for 5G mobile applications," *IEEE Access*, vol. 7, pp. 82288–82296, 2019.
[27] J. Guo, L. Cui, C. Li, and B. Sun, "Side-edge frame printed eight-port dual-band antenna array for 5G smartphone applications," *IEEE Trans. Antennas Propag.*, vol. 66, no. 12, pp. 7412–7417, Dec. 2018.
[28] D. Q. Liu, M. Zhang, H. J. Luo, H. L. Wen, and J. Wang, "Dual-band platform-free PIFA for 5G MIMO application of mobile devices," *IEEE Trans. Antennas Propag.*, vol. 66, no. 11, pp. 6328–6333, Nov. 2018.
[29] W. Jiang, Y. Cui, B. Liu, W. Hu, and Y. Xi, "A dual-band MIMO antenna with enhanced isolation for 5G smartphone applications," *IEEE Access*, vol. 7, pp. 112554–112563, 2019.
[30] K.-L. Wong, C.-Y. Tsai, and J.-Y. Lu, "Two asymmetrically mirrored gap-coupled loop antennas as a compact building block for eight-antenna MIMO array in the future smartphone," *IEEE Trans. Antennas Propag.*, vol. 65, no. 4, pp. 1765–1778, Apr. 2017.
[31] H. Wang and G. Yang, "Compact and low-profile eight-element loop antenna array for the 3.6-GHZ MIMO operation in the future smartphone applications," in *Proc. 6th Asia–Pacific Conf. Antennas Propag. (APCAP)*, Xi'an, China, Oct. 2017, pp. 1–3.
[32] Z. Qin, M. Zhang, J. Wang, and W. Geyi, "Printed eight-element MIMO system for compact and thin 5G mobile handest," *Electron. Lett.*, vol. 52, no. 6, pp. 416–418, Mar. 2016.
[33] J. Li, X. Zhang, Z. Wang, X. Chen, J. Chen, Y. Li, and A. Zhang, "Dual-band eight-antenna array design for MIMO applications in 5g mobile terminals," *IEEE Access*, vol. 7, pp. 71636–71644, 2019.
[34] A. A. Al-Hadi, J. Ilvonen, R. Valkonen, and V. Viikari, "Eight-element antenna array for diversity and MIMO mobile terminal in LTE 3500 MHz band," *Microw. Opt. Technol. Lett.*, vol. 56, no. 6, pp. 1323–1327, Jun. 2014.
[35] Y.-L. Ban, C. Li, C.-Y.-D. Sim, G. Wu, and K.-L. Wong, "4G/5G multiple antennas for future multi-mode smartphone applications," *IEEE Access*, vol. 4, pp. 2981–2988, 2016.
[36] K.-L. Wong and J.-Y. Lu, "3.6-GHz 10-antenna array for MIMO operation in the smartphone," *Microw. Opt. Technol. Lett.*, vol. 57, no. 7, pp. 1699–1704, Jul. 2015.
[37] K.-L. Wong, J.-Y. Lu, L.-Y. Chen, W.-Y. Li, and Y.-L. Ban, "8-antenna and 16-antenna arrays using the quad-antenna linear array as a building block for the 3.5-GHz LTE MIMO operation in the smartphone," *Microw. Opt. Technol. Lett.*, vol. 58, no. 1, pp. 174–181, Jan. 2016.
[38] M.-Y. Li, Z.-Q. Xu, Y.-L. Ban, C.-Y.-D. Sim, and Z.-F. Yu, "Eight-port orthogonally dual-polarised MIMO antennas using loop structures for 5G smartphone," *IET Microw., Antennas Propag.*, vol. 11, no. 12, pp. 1810–1816, Sep. 2017.
[39] X. Zhang, Y. Li, W. Wang, and W. Shen, "Ultra-wideband 8-port MIMO antenna array for 5G metal-frame smartphones," *IEEE Access*, vol. 7, pp. 72273–72282, 2019.
[40] M. S. Khan, F. Rigobello, B. Ijaz, E. Autizi, A. D. Capobianco, R. Shubair, and S. A. Khan, "Compact 3-D eight elements UWB-MIMO array," *Microw Opt Technol Lett*, vol. 60, no. 8, pp. 1967–1971, Aug. 2018.
[41] R. Mathur and S. Dwari, "8-port multibeam planar UWB-MIMO antenna with pattern and polarisation diversity," *IET Microw., Antennas Propag.*, vol. 13, no. 13, pp. 2297–2302, Oct. 2019.
[42] D. Sipal, M. P. Abegaonkar, and S. K. Koul, "Easily extendable compact planar UWB MIMO antenna array," *IEEE Antennas Wireless Propag. Lett.*, vol. 16, pp. 2328–2331, 2017.
[43] R. Saleem, M. Shafique, K. Bajwa, and M. Bilal, "Eight-element UWB-MIMO array with three distinct isolation mechanisms," *Electron. Lett.*, vol. 51, no. 4, pp. 311–313, Feb. 2015.
[44] *CST*. Accessed: Feb. 2018. [Online]. Available: https://www.cst.com/
[45] *ANSYS HFSS*. Accessed: Apr. 2019. [Online]. Available: http://www.ansys.com/

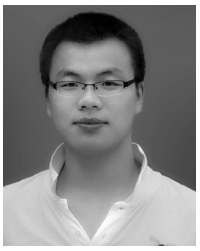

HONGWEI WANG was born in Fengcheng, China. He received the B.S. degree in communication engineering from the Jiangxi University of Finance and Economics, Nanchang, China, in 2012, and the M.S. degree in electromagnetic field and microwave technology from Shanghai University, Shanghai, China, 2015, where he is currently pursuing the Ph.D. degree in electromagnetic field and microwave technology.

His current research interests include LTE multiband MIMO antennas design for smartphone applications, sub 6-GHz multiband MIMO antennas for 5G mobile terminals, and multiband MIMO antenna systems for 4G/5G multimode smartphone applications.

RUIHENG ZHANG was born in Shanghai, China, in 1995. He received the B.S. degree in communication engineering from Shanghai University, Shanghai, in 2018, where he is currently pursuing the M.S. degree in electronics and communication engineering with the School of Communication and Information Engineering. His current research interest includes antenna and RF technology for base stations and terminals for fifth-generation (5G) communications.

YONG LUO received the Ph.D. degree from The University of Tokyo. He was involved in active metamaterial (MTM) for scanning radiation beams by using micro-machining fabrication process to monolithically integrate antennas with MEMS. He is currently an Assistant Professor with Shanghai University (SHU) with the Department of Electronic and Information Engineering and the Shanghai Institute for Advanced Communication and Data Science (SICS). Before joining SHU, he held a postdoctoral position at UCSD. His research interests include active MTM antennas and mmWave antennas.

GUANGLI YANG received the B.S. degree in physics from the Beijing University of Science and Technology, China, in 1997, and the Ph.D. degree in electrical engineering from the University of South Carolina, Columbia, SC, USA, in 2005.

He was mostly with the Antenna and RF Research Group, Motorola Inc., Chicago, IL, USA, from 2005 to 2013, where he started as a Senior Staff and promoted as a Principal Engineer, before he left the company. After that, he has been a Professor with Shanghai University, since March 2014. He is the Director of the EmSensing Group, Shanghai University. He is the author or coauthor of more than 80 publications. He holds over 21 patents filed or issued. His research interests include antennas, phased arrays and digital beam-forming systems for mobile terminals, small cells, radars, and microwave sensing applications. He was the Winner of the Eastern Scholarship Award, in 2013. He was an advisor of high-tech companies.